Imidazole and Imidazolate Iron Complexes: On the Way for Tuning 3D-Structural Characteristics and Reactivity. Redox Interconversions Controlled by Protonation State

ARTICLE *in* INORGANIC CHEMISTRY · AUGUST 2004

Impact Factor: 4.76 · DOI: 10.1021/ic0498687 · Source: PubMed

8 AUTHORS, INCLUDING:

François Lambert
Pierre and Marie Curie University - Paris 6
36 PUBLICATIONS **609** CITATIONS
SEE PROFILE

Stéphanie Durot
University of Strasbourg
25 PUBLICATIONS **524** CITATIONS
SEE PROFILE

Hafsa Korri-Youssoufi
Université Paris-Sud 11
80 PUBLICATIONS **1,419** CITATIONS
SEE PROFILE

Bineta Keita
Université Paris-Sud 11
281 PUBLICATIONS **8,400** CITATIONS
SEE PROFILE

Inorg. Chem. **2004**, *43*, 4178–4188

Imidazole and Imidazolate Iron Complexes: On the Way for Tuning 3D-Structural Characteristics and Reactivity. Redox Interconversions Controlled by Protonation State

François Lambert,*,† Clotilde Policar,*,† Stephanie Durot,† Michèle Cesario,‡ Lu Yuwei,§ Hafsa Korri-Youssoufi,† Bineta Keita,§ and Louis Nadjo§

Laboratoire de Chimie Bio-organique et Bio-inorganique, UMR8124, Institut de Chimie Moléculaire d'Orsay, Bâtiment 420, Université Paris XI, F-91405 Orsay Cedex, France, Institut de Chimie des Substances Naturelles, CNRS, 91198 Gif-sur-Yvette, France, and Laboratoire d'Electrochimie et de Photoélectrochimie, Bâtiment 420, Université Paris-Sud, 91405 Orsay, France

Received February 2, 2004

X-ray structures for six Fe(II) and Fe(III) complexes from two closely heptadentate N-tripodal ligands, $L1H_3$ = tris[(imidazol-4-yl)-3-aza-3-butenyl]amine and $L2H_3$ = tris[(imidazol-2-yl)-3-aza-3-butenyl]amine, are described: three complexes in the L1 series (namely, $[Fe(II)(L1H_3)]^{2+}$ and $[Fe(III)(L1H_3)]^{3+}$ at low pH and $[Fe(III)(L1)]^0$ at high pH) and three complexes in the L2 series (namely, $[Fe(II)(L2H_3)]^{2+}$ at low pH and $[Fe(II)(L2H)]^0$ and $[Fe(III)(L2)]^0$ at high pH). Most of these complexes are stable in both Fe(II) and Fe(III) redox states and with the ligand in various protonation states. In the solid state, hydrogen bonds networks were obtained. Structural differences induced by 2- or 4-imidazole substitution are described and discussed. In solution, interconversions between different forms, with regard to oxidation and protonation states, were investigated by UV–visible spectroscopy, cyclic voltammetry, and potentiometry. The deprotonation pattern of these polyimidazole iron(II) and iron(III) complexes is described in detail. pK_as of the imidazolate/imidazole moieties in MeOH/H_2O are reported. Two new species, namely, $[Fe(II)(L1)]^-$ and $[Fe(II)(L2)]^-$, were shown to be obtained in DMSO upon strong base addition and characterized by UV–vis spectroscopy and cyclic voltammetry. Half-wave potentials of Fe(III)/Fe(II) complexes with ligand moieties in several protonation states are reported, both in DMSO and in MeOH/H_2O. Because of the presence of free imidazole groups coordinated to the iron, the potential of the iron(III)/iron(II) couples can be tuned by pH. A shift of $\Delta E = E_{deprot} - E_{prot}$ ranging from −270 to −320 mV per exchanged proton in DMSO was measured. This study shows moreover that interconversions (with regard to both redox and protonation states) can be reversed several times. As the complexes have been isolated in order to be tested as superoxide dismutase mimics, preliminary reactions with dioxygen and with superoxide, considered as oxidant and reducer of biological importance, are reported. In these two series, O_2^- behaves either as a base or as a reducer and no adducts have been observed.

Introduction

Histidyl imidazole ligand is probably one of the most common ligands encountered at metalloenzyme active sites, and its acidobasic behavior is certainly of first importance in the control of catalytic activity of these enzymes. A better understanding of such a fine-tuning can be provided by the study of model complexes. Iron porphyrins bearing axial imidazole and/or imidazolate have been studied in order to understand the effect of hydrogen bonding[1,2] or the deprotonation[3] of an axial imidazole on the redox potential of the iron(III)/iron(II) couple. Recently this topic has been extended to the study of non-porphyrinic complexes.[3−7] Deprotonation of a coordinated imidazole has also been shown, by us and others, to be an easy way for spontaneous oligomerization of metal complexes (Fe(II) and -(III),

* Authors to whom correspondence should be addressed. E-mail: flambert@icmo.u-psud.fr (F.L.); cpolicar@icmo.u-psud.fr (C.P.). Fax (international): 0033169157231. Tel (international): 0033169154725.
† Université Paris XI.
‡ CNRS.
§ Université Paris-Sud.

(1) Quinn, R.; Mercer-Smith, J.; Burstyn, J. N.; Valentine, J. S. *J. Am. Chem. Soc.* **1984**, *106*, 4136−4144.
(2) O'Brien, P.; Sweigart, D. A. *Inorg. Chem.* **1985**, *24*, 1405−1409.
(3) Quinn, R.; Strouse, C. E.; Valentine, J. S. *Inorg. Chem.* **1983**, *22*, 3934−3940.

10.1021/ic0498687 CCC: $27.50
Published on Web 06/17/2004

Scheme 1. Structure of the Two Ligands $L1H_3$ and $L2H_3$

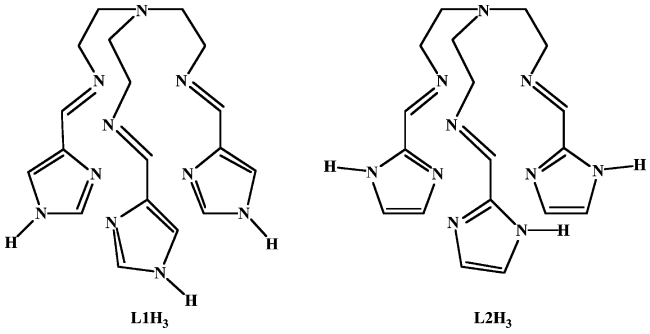

Co(III), Cu(II), Ni(II), ...) into helical chains or bidimensional polymers (see for example refs 8−18).

In our lab, we are producing and studying superoxide dismutase mimics.[19−23] For such activities, the role of protons is essential, as they are necessary for the reduction of superoxide in peroxide.

We are presenting here two iron complex series from two N-centered tripodal potentially heptadentate ligands, tris-[(imidazol-4-yl)-3-aza-3-butenyl]amine (L_1H_3)[14,16] and tris-[(imidazol-2-yl)-3-aza-3-butenyl]amine (L_2H_3) (see Scheme 1).[13] Six X-ray structures in the solid state have been solved involving both ligands in several protonation states.[24] Structural differences induced by 2- and 4-imidazole substitution are discussed.[25] Conversions between the different species (with regard to both redox and protonation states) including two anionic forms, namely, $[Fe(II)(L1)]^-$ and $[Fe(II)(L2)]^-$, are presented. Dependence of iron(III)/iron(II) redox potential on protonation state of the imidazolate/imidazole moiety is studied. The two families showed similar behavior. Moreover, preliminary results (i) on the reaction of superoxide with these iron(III) and iron(II) complexes and (ii) on the reaction of dioxygen with one of these iron(II) complexes are presented.

Experimental Section

Materials. $FeCl_2 \cdot 4H_2O$ and $FeCl_3 \cdot 6H_2O$ were purchased from Across; $Fe(ClO_4)_2 \cdot H_2O$, $Fe(ClO_4)_3 \cdot H_2O$, (imidazol-2-yl)carboxaldehyde (97%), and tris(2-aminoethyl)amine (TREN) from Aldrich and used without further purification. Diethyl ether and methanol were dried respectively on sodium−benzophenone and magnesium. For electrochemical measurements, high quality grade chemicals were purchased from Aldrich (DMSO (99.8%, water <0.005%), Bu_4NPF_6, KCl).

Physical Measurements. Electronic absorption spectra were recorded on a Safas 190 DES spectrophotometer at room temperature with quartz cells. Infrared spectra were recorded on a IFS 66 Fourier transform infrared Bruker spectrometer using KBr pellets. ^1H and ^{13}C NMR spectra of the ligands and complexes were recorded on AC 200 and AC 250 Bruker spectrometers using deuterated solvents. Mass spectra in the positive mode were obtained with a time-of-flight (PDMS) mass spectrometer fitted with a ^{252}Cf source.

Electrochemical Experiments. Bu_4NPF_6 (supporting electrolyte) was dried at 80 °C under vacuum for 3 days. The solutions were deaerated thoroughly for at least 30 min with pure argon and kept under a positive pressure of this gas during the experiments. The electrochemical experiments were performed in a three compartment cell at room temperature using dry dimethyl sulfoxide, 0.1 mol L^{-1} Bu_4NPF_6. The reference electrode was a saturated calomel electrode (SCE), separated from the test solution by an intermediate bridge containing the supporting electrolyte and closed by a fine porosity ceramic frit. The counter electrode was a platinum gauze soaked in the supporting electrolyte, and separated from the test solution by a medium porosity glass frit. The working electrode was a 3 mm diameter glassy carbon disk (GC, Tokai, Japan). Its mounting and polishing have been previously described.[26] The electrochemical setup was an EG$G273A potentiostat driven by a PC with the EG$G270 software. In CH_3OH/H_2O (2/1), KCl 0.1 mol L^{-1} was used as an electrolyte support and pH was directly measured in the electrochemical cell. Typically, complexes were used as 10^{-3} mol L^{-1} solutions.

Complexes. Crystal Data, Data Collection, and Refinements. Relevant information for recording and refinement of the six crystal

(4) Haga, M.-a.; Ano, T.-a.; Kano, K.; Yamabe, S. *Inorg. Chem.* **1991**, *30*, 3843−3849.
(5) Deroche, A. *Complexes métalliques modèles de superoxyde dismutases à fer ou à managnèse: synthèse, structure, propriétés physico-chimiques et réactivité*. University Paris XI, Orsay, 1995.
(6) Carina, R. F.; Verzegnassi, L.; Bernadinelli, G.; Williams, A. F. *Chem. Commun.* **1998**, 2681−2682.
(7) Brewer, C.; Brewer, G.; Luckett, C.; Marbury, G. S.; Viragh, C.; Beatty, A. M.; Scheidt, R. W. *Inorg. Chem.* **2004**, *43*, 2402−2415.
(8) Matsumoto, N.; Mizuguchi, Y.; Mago, G.; Eguchi, S.; Myiasaka, H.; Nakashima, T.; Tuchagues, J.-P. *Angew. Chem., Int. Ed. Engl.* **1997**, *36*, 1860−1861.
(9) Myiasaka, H.; Okumara, S.; Nakashima, T.; Matsumoto, N. *Inorg. Chem.* **1997**, *36*, 4329−4335.
(10) Brewer, C. T.; Brewer, G.; Shang, M.; Scheidt, R. W.; Muller, I. *Inorg. Chim. Acta* **1998**, *278*, 197−201.
(11) Mimura, M.; Matsuo, T.; Motoda, Y.; Matsumoto, N.; Nakashima, T.; Kojima, M. *Chem. Lett.* **1998**, 691−692.
(12) Katsuki, I.; Matsumoto, N.; Kojima, M. *Inorg. Chem.* **2000**, *39*, 3350−3354.
(13) Lambert, F.; Renault, J.-P.; Policar, C.; Morgenstern-Badarau, I.; Cesario, M. *Chem. Commun.* **2000**, 35−36.
(14) Sunatsuki, Y.; Sakata, M.; Matsuzaki, S.; Matsumoto, N.; Kojima, M. *Chem. Lett.* **2001**, 1254−1255.
(15) Katsuki, I.; Motoda, Y.; Sunatsuki, Y.; Matsumoto, N.; Nakashima, T.; Kojima, M. *J. Am. Chem. Soc.* **2002**, *124*, 629−640.
(16) Sunatsuki, Y.; Ikuta, Y.; Matsumoto, N.; Ohta, H.; Kojima, M.; Iijima, S.; Hayami, S.; Maeda, Y.; Kaizaki, S.; Dahan, F.; Tuchagues, J.-P. *Angew. Chem., Int. Ed.* **2003**, *42*, 1614−1618.
(17) Ikuta, Y.; Ooidemizu, M.; Yamahata, Y.; Masahiro, Y.; Shutaro, O.; Matsumoto, N.; Iijima, S.; Sunatsuki, Y.; Kojima, M.; Dahan, F.; Tuchagues, J.-P. *Inorg. Chem.* **2003**, *42*, 7001−7017.
(18) Yamada, M.; Ooidemizu, M.; Ikuta, Y.; Osa, S.; Matsumoto, N.; Iijima, S.; Kojima, M.; Dahan, F.; Tuchagues, J.-P. *Inorg. Chem.* **2003**, *42*, 8406−8416.
(19) Deroche, A.; Morgenstern-Badarau, I.; Cesario, M.; Guilhem, J.; Keita, B.; Nadjo, L.; Houée-Levin, C. *J. Am. Chem. Soc.* **1996**, *118*, 4567−4573.
(20) Rodriguez, M. C.; Morgenstern-Badarau, I.; Cesario, M.; Guilhem, J.; Keita, B.; Nadjo, L. *Inorg. Chem.* **1996**, *35*, 7804−7810.
(21) Rodriguez, M. C.; Lambert, F.; Cesario, M.; Morgenstern-Badarau, I. *Inorg. Chem.* **1997**, *36*, 3525−3531.
(22) Morgenstern-Badarau, I.; Lambert, F.; Deroche, A.; Cesario, M.; Guilhem, J.; Keita, B.; Nadjo, L. *Inorg. Chim. Acta* **1998**, *275*−*276*, 234−241.
(23) Policar, C.; Durot, S.; Cesario, M.; Lambert, F.; Ramiandrasoa, F.; Morgenstern-Badarau, I. *Eur. J. Inorg. Chem.* **2001**, 1807−1817.

(24) While this manuscript was under revision, a paper appeared in *Inorg. Chem.* by Brewer et al. (ref 7) describing structurally three of the complexes, crystallized here with different counteranion. In this paper, only the structure of the entirely new [Fe(II)(L2H)] complex is detailed. To avoid any redundancy, other structural data have been moved to the Supporting Information. However, complex preparations are reported in the Experimental Section as different counteranions have been used.
(25) Spin states for similar compounds have been published elsewhere (see refs 7, 10, 13, 14, 16, 17, 18). A systematic investigation of spin state equilibrium by Mössbauer spectroscopy can be found in Brewer's article (see ref 7). We have thus chosen to not focus on spin states here.
(26) Keita, B.; Essadi, K.; Nadjo, L. *J. Electroanal. Chem.* **1989**, *259*, 127.

structures are reported in the Supporting Information. Structural data have been deposited at the Cambridge Crystallographic Data Centre, and CCDC numbers are given below.

Single crystals were mounted on a Enraf-Nonius CAD4 diffractometer with graphite monochromated Mo Kα radiation ($\lambda = 0.7107$ Å). The data collections were all performed at room temperature. Three standard reflections were measured every 3 h, to monitor instrument and crystal stability. No significant decay was observed. Data were corrected for Lorentz and polarization factors but not for absorption. Structures were solved by direct methods (SHELXS86)[27] and refined anisotropically on F^2 for all reflections by least-squares methods using SHELXL-93.[28] Hydrogen atoms were included in the refinement at their ideal position and assigned an isotropic thermal parameter of 1.2 that of the bonded atoms.

[Fe(II)(L1H$_3$)](PF$_6^-$)$_{1.5}$(H$_7$O$_4^-$)$_{0.5}$ (Orange).[29] A solution of $FeCl_2 \cdot 4H_2O$ (66 mg, 0.33 mmol) in degassed dry methanol (5 mL) was slowly added to a methanolic solution (10 mL) of ($L1H_3$) (125 mg, 0.33 mmol). The resulting orange solution was stirred for 10 min, and NH_4PF_6 (134 mg, 0.82 mmol) in methanol (5 mL) was added. The complex was crystallized as orange hexagonal plates from the methanolic solution by diffusion of diethyl ether. Crystals were unstable over drying. Anal. Calcd for [C_{18} $H_{27.5}N_{10}O_2FeP_{1.5}F_9$]-($H_2O$)$_{0.3}$: H 4.08, C 31.12, P 6.69, Fe 8.04. Found: H 4.33, C 31.23, P 6.25, Fe 7.44. IR: ν (C═N) 1638 cm^{-1}, (C═C and C═N imidazoles) 1507 and 1444.5 cm^{-1}, ν (PF_6^-) 842 and 555 cm^{-1}. UV−visible in DMSO, λ (nm) (ϵ (L mol^{-1} cm^{-1})): 261 (35890), 454 (1974). Structural data deposited at the Cambridge Crystallographic Data Centre CCDC No. 228881.

[Fe(II)(L2H$_3$)] (PF$_6^-$)$_{1.5}$ (Cl$^-$)$_{0.5}$ (H$_2$O)$_2$ (Red). A solution of $FeCl_2 \cdot 4H_2O$ (66 mg, 0.33 mmol) in degassed dry methanol (5 mL) was slowly added to a methanolic solution (10 mL) of ($L2H_3$) (125 mg, 0.33 mmol) at 40 °C. The resulting dark red solution was stirred for 10 min, and NH_4PF_6 (134 mg, 0.82 mmol) in methanol (5 mL) was added. Diethyl ether diffusion in the resulting solution provided beautiful thick dark red crystals suitable for X-ray analysis. Anal. Calcd for [$C_{18}H_{24}N_{10}Fe_1(PF_6)_{1.5}(Cl)_{0.5}$]($H_2O$)$_2$: C 30.56, H 3.99, N 19.8, Cl 2.51, Fe 7.89. Found: C 30.46, H 3.93, N 19.34, Cl 3.21. IR in KBr: ν (C═N) 1628 cm^{-1}, (C═C and C═N imidazoles) 1464 and 1438 cm^{-1}, (PF_6^-) 841 and 558 cm^{-1}. UV−visible in water/methanol (3/1), λ (nm) (ϵ (L mol^{-1} cm^{-1})): 500 (1600) and 275 (29000).

[Fe(III)(L1H$_3$)](PF$_6^-$)$_2$(Cl$^-$)$_1$ (Red). A solution of $FeCl_3 \cdot 6H_2O$ (180 mg, 0.66 mmol) in degassed dry methanol (5 mL) was slowly added to a methanolic solution (10 mL) of (L1H3) (125 mg, 0.33 mmol). The resulting dark red solution was stirred for 10 min, and NH_4PF_6 (265 mg, 1.6 mmol) in methanol (5 mL) was added. Little red hexagonal crystals were obtained within 3 h. Thick crystals suitable for X-ray structure analysis were grown by diffusion of ethyl acetate in the mother liquor. Crystals were air stable. Anal. Calcd for [$C_{18}H_{24}N_{10}FeP_2F_{12}Cl$]($H_2O$): C 27.73, H 3.36, N 17.96, P 7.95, Fe 7.16. Found: C 27.53, H 3.09, N 17.54, P 8.34, Fe 7.04. UV−visible in water/methanol (3/1), λ (nm) (ϵ (L mol^{-1} cm^{-1})): 518 (2990); 340 (3190) and 258 (38950). Structural data deposited at the Cambridge Crystallographic Data Centre CCDC No. 228883.

[Fe(III)(L$_1$)](PF$_6^-$)$_{0.5}$[(H$_9$O$_4$)$^+$]$_{0.5}$ (Blue).[29] A solution of $FeCl_3 \cdot 6H_2O$ (180 mg, 0.66 mmol) in degassed dry methanol (5 mL) was slowly added to a methanolic solution (10 mL) of (L1H3) (125 mg, 0.33 mmol). The resulting dark red solution was stirred for 10 min, and NH_4PF_6 (54 mg, 0.33 mmol) in methanol (5 mL) was added. A solution of sodium methanolate in methanol was added to obtain a deep blue solution. Blue hexagonal crystals were formed by diffusion of ethyl acetate in the resulting blue solution. Crystals were suitable for X-ray structure analysis and air stable. Anal. Calcd for [$C_{18}H_{25.5}N_{10}O_2FeP_{0.5}F_3$]($H_2O$): C 38.59, H 4.95, N 25, P 2.76, Fe 9.97. Found: C 38.97, H 4.74, N 24.81, P 3.08, Fe 10.14. IR: ν (C═N) 1586, ν (PF_6^-) 842 and 558 cm^{-1}. UV−visible in methanol, λ (nm) (ϵ (L mol^{-1} cm^{-1}): 292 (40829); 618 (2050). Structural data deposited at the Cambridge Crystallographic Data Centre CCDC No. 228435.

[Fe(III)(L$_2$)](H$_2$O)$_{4.5}$ (Blue). [Fe(II)($L2H_3$)](PF$_6^-$)$_{1.5}$(Cl$^-$)$_{0.5}$(H_2O)$_2$ was dissolved in a mixture (water/methanol) (1/1). To this red solution was added NaOH (0.1 mol L^{-1}) up to pH 11 under aerobic conditions. The deep blue resulting solution was slowly evaporated, leading to blue hexagonal crystals. The same crystals can be obtained by diffusion of ethyl acetate in the blue methanol solution prepared by addition of sodium methanolate in a methanolic solution of [Fe(II)($L2H_3$)](PF$_6^-$)$_{1.5}$(Cl$^-$)$_{0.5}$(H_2O)$_2$. Crystals were air instable by loss of solvent but were suitable for X-ray structure determination. Microanalysis was consistent with the loss of 1.5 H_2O per iron (by comparison to X-ray structure). Anal. Calcd for [$C_{18}H_{21}N_{10}$-Fe](H_2O)$_3$: C 44.36, H 5.58, N 28.74, Fe 11.46. Found: C 44.53, H 5.40, N 29.09, Fe 11.46. IR in KBr: ν (C═N) 1580 cm^{-1}, C═C and C═N imidazoles) 1464 and 1438 cm^{-1}, (PF_6^-) 841 and 558 cm^{-1}. UV−visible in methanol, λ (nm) (ϵ (L mol^{-1} cm^{-1})): 292 (29000); 618 (2800). Structural data deposited at the Cambridge Crystallographic Data Centre CCDC No. 229006.

[Fe(II)(L2H$_1$)](H$_2$O)$_1$ (Pink). Under argon pressure, the complex [Fe(II)(L_2H_3)] (PF$_6^-$)$_{1.5}$ (Cl$^-$)$_{0.5}$(H_2O)$_2$ (50 mg) was dissolved in deoxygenated methanol. A methanolic solution of NaOH (0.1 mol L^{-1}) and 0.1 equiv of a methanol solution of sodium ascorbate was added to this red solution. The deep red-pink solution was filtrated under argon and slowly evaporated, under argon flow, to form pink hexagonal crystals. Crystals were air stable enough to be suitable for X-ray structure determination. Only 15 mg of crystalline product was obtained, and only an X-ray structure was provided. Structural data deposited at the Cambridge Crystallographic Data Centre CCDC No. 229007.

A summary of crystal data, intensity measurements, and structure refinement for complexes from L1 and L2, except for [Fe(II)(L2H)] (see below), can be found in the Supporting Information.

Mass Spectra. All the complexes present the same (PDMS) mass spectrum with three major peaks at $M = 217.5$ (100%) [Fe(L)]$^{2+}$, 435 (65%) [Fe(L)]$^+$, 870 (15%) [2(Fe(L))]$^+$.

Acid−Base Titration. Direct Titration. Each titration was done in a MeOH/H_2O (2/1) solution on a 10^{-2} mol L^{-1} complex solution. [Fe(II)($L2H_3$)]$^{2+}$ was titrated upward by NaOH (0.09 mol L^{-1})/ascorbate (0.01 mol L^{-1}) from pH 5.8 to 12 and downward to pH 2.2 by HCl (0.1 mol L^{-1}). [Fe(II)($L1H_3$)]$^{2+}$ was titrated by HCl (0.1 mol L^{-1}) from pH 5.9 to 2.2. [Fe(III)(L2)]^0 and [Fe(III)(L1)]^0 were titrated by HCl (0.1 mol L^{-1}) from pH 8.5 to 2.2. [Fe(III)-($L1H_3$)]$^{3+}$ was titrated by HCl (0.1 mol L^{-1}) from pH 5.8 to 1.5.

pK_a Determination. The number of exchanged protons (x) (see Figure 6) was determined using the formula $x = ((n_{acid} - n_{H^+}) - (n_{base} - n_{OH}))/n_{reagent}$, where n_{acid} (HCl) is the number of moles of acid added, n_{base} (NaOH) is the number of moles of base added, n_{H^+} and n_{OH} are the numbers of moles of H^+ and OH^- in solution recalculated from the pH value, and $n_{reagent}$ is the mole number of complex that is titrated. $x > 0$ indicates the number of protons that has been added to the reagent. The variation of x as a function of

(27) Sheldrick, G. M. University of Göttingen, Germany, 1986.
(28) Sheldrick, G. M. *Program for the refinement of crystal structures*; University of Göttingen: Göttingen, Germany, 1993.
(29) ($H_7O_4^-$)$_{0.5}$ is equivalent to $3H_2O + 1OH^-$. ($H_9O_4^+$)$_{0.5}$ is equivalent to $3H_2O + 1H_3O^+$. They constitute the "four-oxygen units" (see below in the text.)

Table 1. Summary of Crystal Data, Intensity Measurements, and Structure Refinement for [Fe(II)(L2H)] Complex

formula (asym unit)	$[Fe_{0.67}C_{12}N_{6.67}H_{14.66}]\cdot 0.67H_2O$	D_c, Mg m^{-3}	1.482
name	$[Fe(II)(L2H)]^0$	μ(Mo Kα), mm^{-1}	0.778
color	pink	cryst size, mm	0.06 × 0.06 × 0.5
mol wt	452.32	no. of reflns measd	3521
cryst syst	trigonal	θ range deg	2.08 to 24.96
space group	*P*31*c*	*hkl* ranges	$-12 \le h \le 11$, $-2 \le k \le 12$, $0 \le l \le 23$
a, Å	10.939(5)	no. of unique reflns	1232 [*R*(int) = 0.0572]
b, Å	10.939(5)	no. of reflns obsd $I > 2\sigma(I)$	3520
c, Å	19.558(8)	no. of params/restraints	1219/121
α, β, deg	90	final *R* indices	R1 = 0.0371
γ, deg	120	R1 [$I > 2\sigma(I)$]	[725 data]
V, Å^3	2026.8	wR2	0.0953
Z	4	largest diff peak and hole, e/Å^3	0.31, −0.53
F(000)	944		

$[H^+]$ was fitted with the formula for a tetrabase, as in the example, to provide pK_as:

$$x = \{4[H^+]^4 + 3K_{a1}[H^+]^3 + 2K_{a1}K_{a2}[H^+]^2 + K_{a1}K_{a2}K_{a3}[H^+]\}/\{[H^+]^4 + K_{a1}[H^+]^3 + K_{a1}K_{a2}[H^+]^2 + K_{a1}K_{a2}K_{a3}[H^+] + K_{a1}K_{a2}K_{a3}K_{a4}\} - x_0$$

(x_0 being the number of protons on the complex before acid addition).

Spectrophotometric Characterization of [Fe(II)(L)]$^-$ by UV−Vis Spectroscopy and Electrochemistry. The UV−vis spectrum of the complex $[Fe(II)(L2)]^-$ (respectively $[Fe(II)(L1)]^-$) in DMSO was obtained upon addition of excess of tBuOK in a 5×10^{-4} mol L^{-1} $[Fe(II)(L2H_3)]^{2+}$ solution (respectively $[Fe(II)(L1H_3)]^{2+}$) under argon {compound, color, λ (nm), ϵ (mol^{-1} L cm^{-1}): $[Fe(II)(L2)]^-$, purple, (552, 3600 ± 80); $[Fe(II)(L1)]^-$, pink, (506, 2300 ± 50)}.

Redox couple ($[Fe(III)(L2)]/[Fe(II)(L2)]^-$) (respectively ($[Fe(III)(L1)]/[Fe(II)(L1)]^-$)) was characterized by cyclic voltammetry upon addition of tBuOK in a 10^{-3} mol L^{-1} $[Fe(II)(L2H_3)]^{2+}$ solution (respectively $[Fe(II)(L1H_3)]^{2+}$) (see Figure 8) {redox couple, $E_{1/2}$ (mV/SCE): ($[Fe(III)(L1)]/[Fe(II)(L1)]^-$), −445; ($[Fe(III)(L2)]/[Fe(II)(L2)]^-$), −457}.

Kinetics of the Oxidation of [Fe(II)(L2H$_3$)]$^{2+}$ in Basic Medium. A solution (solution A) of $[Fe(II)(L2H_3)]^{2+}$ (5×10^{-5} mol L^{-1}) was prepared in deaerated methanol. Two phosphate buffers (10^{-2} mol L^{-1}, pH 8 and 9) were prepared (solution B) under aerobic conditions. One milliliter of A was introduced at $t = 0$ s in the cell containing 1 mL of B. Initial concentration in dioxygen was measured by polarography (3.8×10^{-4} molL^{-1}). The spectrum was recorded as a function of time (Figure 10). From the absorbances at 284 and 470 nm, the kinetics of the oxidation was quantified. Linear plots for $(\ln (A - A_0)/(A_{inf} - A_0)) = f(t)$ were observed up to 1200 s, and an apparent first-order kinetic constant k_{app} was derived from linearization (see Figure 11 and Table 7).

Reactivity with Superoxide in Anhydrous DMSO. A saturated solution of KO_2 in anhydrous DMSO was prepared as previously described. [23] Incremental equivalents (0 to 3 equiv) of superoxide were added to a solution of $[Fe(III)(L2)]^0$ 4×10^{-4} mol L^{-1} in anhydrous DMSO, and UV−vis spectra were recorded.

Results and Discussion

Polyimidazole ligands $L1H_3$ and $L2H_3$ (see Scheme 1) have been already used in the literature,[7,11,13−15,30] and their characterizations have been very recently published.[7] Depending on the protonation state of the imidazoles, several complexes can be obtained with either Fe(II) or Fe(III). For L1, three complexes have been crystallized and structurally charatacterized in the solid state (see Supporting Information): $[Fe(II)(L1H_3)](PF_6^-)_{1.5}(H_7O_2^-)_{0.5}$, $[Fe(III)(L1H_3)](PF_6^-)_2(Cl^-)_1$, and $[Fe(III)(L1)]^0(PF_6^-)_{0.5}[(H_9O_4)^+]_{0.5}$. For L2, three complexes have been X-ray characterized (see Supporting Information and Table 1): $[Fe(II)(L2H_3)](PF_6^-)_{1.5}(Cl^-)_{0.5}(H_2O)_2$, $[Fe(III)(L_2)](H_2O)_{4.5}$, and $[Fe(II)(L2H_1)](H_2O)_1$, the latter $[Fe(II)(L2H_1)](H_2O)_1$ being entirely new (see Table 1).[24] $[Fe(II)(L1)]^-$ and $[Fe(II)(L2)]^-$ were shown to be obtained in DMSO upon strong base addition. In solution, interconversions driven by proton and/or electron transfer can be monitored either by UV−visible spectroscopy, cyclic voltammetry, or potentiometry. For each family, this study showed that interconversion involving the five different species from Scheme 2 can be reversed several times. Moreover, the reactivity with dioxygen and superoxide, as they are respectively oxidant and reducer of biological importance, has been investigated.

A. Description of the Structures. 1. General Description of Fe−L Units. The structure of $[Fe(III)(L2)]^0$ has been already published by us as part of an alternate polymer $[Fe(III)(L2)]_2[Mn(II)(hfac)_2]_3$.[13] Four of the crystal structures of these iron polyimidazole molecular complexes have been previously described in the literature, but with other counteranions: $[Fe(III)(L1H_3)(ClO_4)_3$,[14] $[Fe(II)(L1H_3)]^{2+}$ as part of an alternate polymer $[Fe(II)(L1H_3)][Fe(III)L1](NO_3)_2$,[16] [Fe(III)(L1)], [Fe(III)(L2)], $[Fe(II)(L2H_3)](ClO_4)_2$.[7] In this work, crystals suitable for X-ray diffraction have been obtained for ionic complexes by partial or complete exchange of chloride for hexafluorophosphate counteranion. Two complexes, namely, $[Fe(II)(L2H)]^0$ and $[Fe(III)(L2)]^0$, are neutral and crystallized without any counteranion.

The two ligands, $L1H_3$ and $L2H_3$, although very similar, allowed different structures when complexed to iron, depending on both the oxidation state of iron and the protonation state of imidazolate. All the complexes are hexacoordinated and display pseudooctaedric geometry around the iron, as exemplified in Figure 1. Selected distances and angles are given in Table 2 for $[Fe(II)(L2H)]^0$ (selected distances and angles for other complexes can be found in the Supporting Information). They are typical for such complexes and their spin state, [7,10,12−14,16,17,22] as reported and discussed by Brewer et al. in a very recent paper describing complete Mössbauer spectroscopy and ligand field analysis for some of these complexes.[7]

(30) Yang, S.-P.; Tong, Y.-X.; Zhu, H.-L.; Cao, H.; Chen, X.-M.; Ji, L.-N. *Polyhedron* **2001**, *20*, 223−229.

Scheme 2. Interconversions between the Different Forms

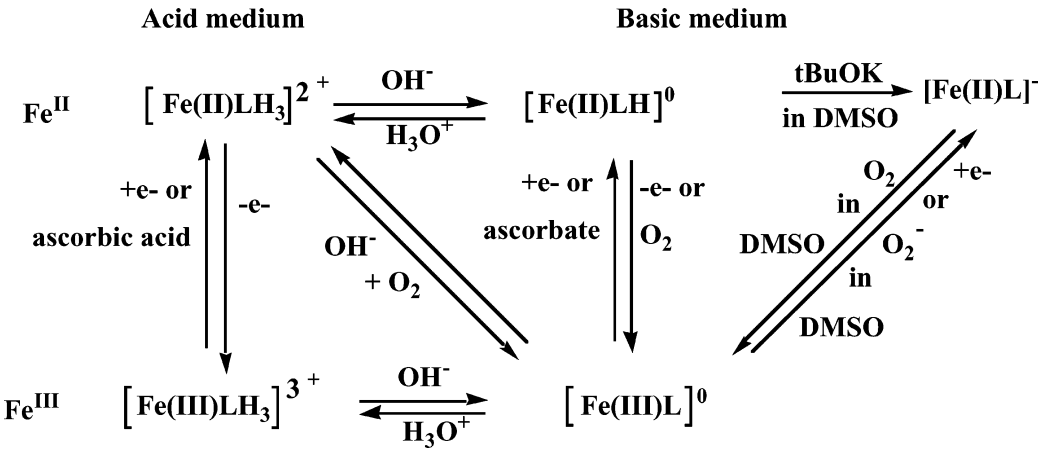

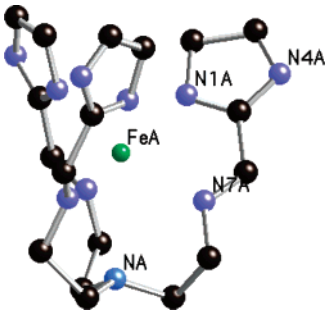

Figure 1. [Fe(II)(L2H)]complex. Hydrogens have been removed for clarity.

Table 2. Selected Distances and Angles for [Fe(II)(L2H)](H_2O) (Pink)[a]

Distances (Å)	
Fe−$N_{tripodal}$	2.98(8)
Fe−N_{7imine}	2.27(2); 2.20(2)
Fe−$N_{1imidazole}$	2.25(2); 2.207(13)
Angles (deg)	
C−$N_{tripodal}$−C	113.3(9); 113.6(11)
N_7−Fe−$N_{7'}$	101.4(4); 100.6(5)
N_1−Fe−$N_{1'}$	86.0(6); 86.7(5)
N_7−Fe−N_1	74.7(6); 74.7(5)

[a] For distances and angles of other complexes, see Supporting Information.

2. Water Networks and Overall Layout of Crystal Structures. For all of these complexes but [Fe(III)($L1H_3$)]-(PF_6^-)$_2$(Cl^-)$_1$ water molecules were found in the crystal structures (1 to 4.5 water molecules per iron). In most cases, water was bound to $N_{imidazole}$. In the case of {[Fe(II)(L2H)]-(H_2O)}, [{Fe(II)($L1H_3$)}],(PF_6^-)$_{1.5}$,($H_7O_4^-$)$_{0.5}$], and [{Fe(III)-(L1)}],(PF_6^-)$_{0.5}$,($H_9O_4^+$)$_{0.5}$], water molecules displayed interesting organizations that are described below, along with 3D layout of the crystal.

{[Fe(II)(L2H)](H$_2$O)}. In the case of the iron(II) complex isolated from L2 under basic conditions, the ratio iron/H_2O was 1. In the solid state, each Fe−L2 unit was linked to three H_2O. Each H_2O was linked to three imidazoles from three different complexes. It resulted in a quite symmetrical structure, as shown in Figure 3. Water molecules were embedded within a layer of Fe-L2 units, consisting of two entangled sublayers, with the capped tripod by alternately up (sublayer labeled B in Figure 2) and down (sublayer labeled A) (see refs 13, 16, and 18 for similar capping up and down). The layers, referred to as (AWB), were perpendicular to the *c*-axis. Within the (AWB) layers, six complexes were organized around two water molecules (W_A−W_B parallel to *c*-axis) on a honeycomb-like network with six Fe−L2 units alternately above (A) and below (B) (see Figure 2). Stacking of the layers resulted in the formation of tunnels parallel to the *c*-axis and perpendicular to the layers. These tunnels were hosting an infinite column of waters (see Figure 3) with an alternate distance d_{O-O} of 4.77 and 5 Å. The 3D structure can be summed up as a pileup of layers {(A−W−B)(A−W−B)}$_n$ perpendicular to the *c*-axis, the dash (−) representing hydrogen bonds connecting water to imidazole. No particular interaction but van der Waals contributed to the piling up of (AWB)$_n$ layers.

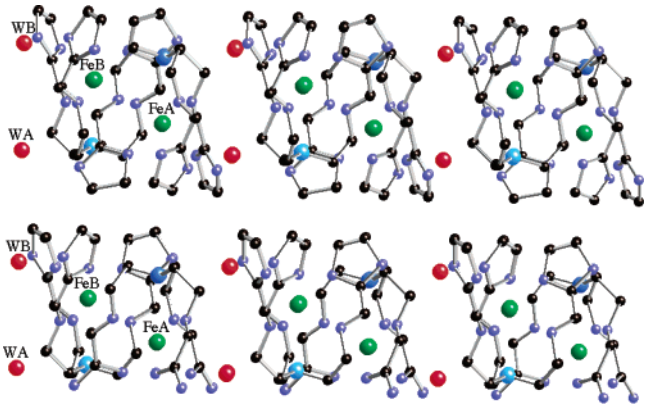

Figure 2. Structure of [Fe(II)(L2H)]^0: piling up of two layers {(A−W−B)(A−W−B)}. W_A is hydrogen bound to $N_{imidazoleA}$ (sublayer A), and W_B is hydrogen bound to $N_{imidazoleB}$ (sublayer B). The *c*-axis is vertical.

[{Fe(II)($L1H_3$)}(PF_6^-)$_{1.5}$($H_7O_4^-$)$_{0.5}$] and [{Fe(III)(L1)}-(PF_6^-)$_{0.5}$($H_9O_4^+$)$_{0.5}$]. For both [{Fe(II)($L1H_3$)}(PF_6^-)$_{1.5}$-($H_7O_4^-$)$_{0.5}$] and [{Fe(III)(L1)}(PF_6^-)$_{0.5}$($H_9O_4^+$)$_{0.5}$], similar uncommon four-water-molecule discrete networks (W1, W2i−iii, from here on referred to as "four-oxygen units") were found with an intriguing structure (see Figure 4A and Figure 4B in the case of the latter). The overall organization involved stacking of alternate water layers (W) and Fe−L1 unit layers, perpendicular to the *c*-axis. In Fe−L1 layers (referred to as AB), a honeycomb-like 2D network of Fe−L1 units was observed. An N-tripodal claw was capping the iron, alternately down the *c*-axis (sublayer A) and up the *c*-axis (sublayer B). W2i, W2ii, and W2iii were connected

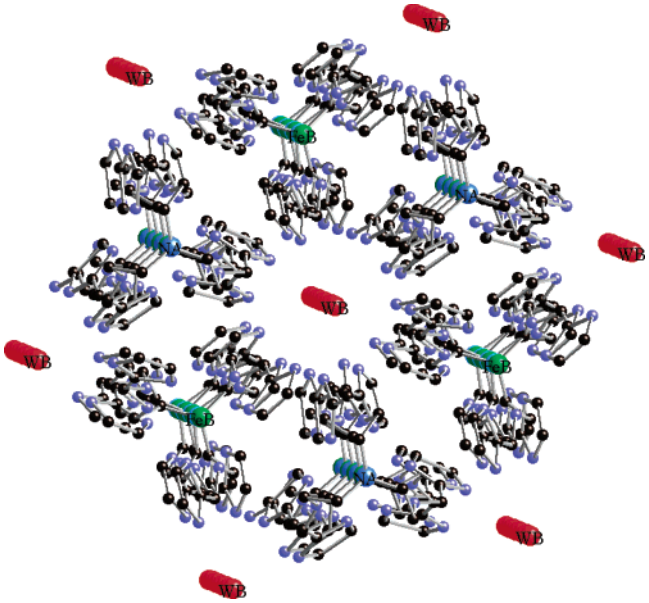

Figure 3. Column of waters in the structure of $[Fe(II)(L2H)]^0$: view along a direction close to the *c*-axis.

to the central W1, located on the 3-fold axis.[31] Each W2 was moreover bound to the Fe−L1 layer just below (AB) and to the Fe−L1 layer just above {(AB)′}, with a hydrogen bond involving three free-imidazole nitrogens (N3) from sublayer A′ and three free-imidazole nitrogens (N3) from sublayer B (Figure 4B).[13,14,17,18] W1 was capped by an N-tripod from sublayer B′ (layer just above) and sublayer A (layer just below).

Figure 4B shows the hexagonal layout around a unique "four-oxygen unit" (W1, W2i−iii), with Fe−L1 belonging to an (AB) layer just below (A′) and to an (AB) layer just above (B). The *mille feuilles* can be described as the stacking of layers perpendicular to the *c*-axis: $\{W-AB-W-AB-\}_n$ with hydrogen bond connections (−) between layers. Scheme 3 shows a schematic view of this 3D layout.

No proton but one—in the case of Fe(III) (HW1)[31]—was crystallographically located. However, their number can be calculated out of charge balance. Over a unit consisting of two Fe centers, six imidazolates, and a four-oxygen unit,[32] 9 protons were found in the case of Fe(III) and 13 protons in the case of Fe(II). Their positions can be guessed from the four-oxygen unit, assuming a hydrogen-bond network connecting W2 to both W1 and N3. Such a network is described in Scheme 4 and Table 3.

A few points are worth noting, for a better understanding of the control over 3D structures. In the first place, the more protons, the larger the "four-oxygen unit" (see distances in Table 3). In the second place, the surprising coplanar four oxygens can be related both to the delocalized hydrogen bond network—over the "four-oxygen unit" and six imidazolates—and to the steric constraint from the capping above and below W1 (see Scheme 3 and Figure 4A).

The importance of hydrogen bonding for the control of the 3-dimensional structure of solids has been previously stressed (see for example refs 11, 13, and 15). This study shows that control over the 3D layout can be achieved through the ligand geometry. Despite very similar structure for the two ligands ($L1H_3$ and $L2H_3$), different overall layouts were obtained here. There is probably a fine-tuning due to the 2-imidazole versus 4-imidazole. With 2-imidazole, as in the L2 series, N_3-H is directed inward toward the Fe−L2 layer. On the contrary, with 4-imidazole, as in the L1 series, N_3-H is pointing outward from the layer (see Scheme 5). This could be used so as to fine-tune 3D-structural characteristics. As an example of such a fine-tuning, it had been previously possible to generate a layered bimetallic Mn(II)-Fe(III) imidazolate 2D polymer from $[Fe(III)(L2)]^0$, whereas no polymer was ever isolated from $[Fe(III)(L1)]^0$.[13]

3. Structure in Solution. The ^1H NMR data of the Fe(II) complexes showed well-resolved peaks at up to 250 ppm typical for high spin Fe(II) complexes. The NMR peak number (7 peaks in CD_3OD, with $HN_{imidazole}$ being exchanged) showed that the C_3 symmetry of neutral or cationic complexes remained in solution, at least at the NMR time scale. It is exemplified in Figure 5 in the case of $[Fe(II)(L2H_3)](PF_6^-)(Cl^-)$. The three imidazole pendent arms were thus equivalent in the complexes. So, we concluded that a very similar pseudooctaedric structure is encountered for Fe−L units (A.1) in the solid state and in solution.

B. Protonation Equilibria. The behavior of iron(II) and iron(III) complexes issued from L1 and L2 was investigated on a large pH scale (from 2 to 12). Both spectrophotometry and cyclic voltammetry were performed at different pH, and potentiometric titrations were used. To enhance solubilities, $MeOH/H_2O$ was used. For $[Fe(II)(L2H_3)]^{2+}$, titration has been done under anaerobic conditions or with ascorbate. In the case of $[Fe(II)(L1H_3)]^{2+}$ a precipitate was obtained[33] under anaerobic conditions upon base addition preventing a similar study (see D.1).

Iron(III)L1. Direct titration of $[Fe(III)(L1)]^0$ with HCl showed two equivalences. The first equivalence was associated with three protons (see Figure 6 and Experimental Section). Three pK_a values were extracted by simulation (see Experimental Section): 9.9, 8.5, 7.3. The second equivalence, associated with a pK_a value of 4.4, corresponded to a fourth proton. This titration was followed by UV−visible spectroscopy (results not shown). It showed one isobestic point at 410 nm and an isobestic area between 620 and 670 nm. The fact that an "area" was observed—and no neat isobestic point—is in agreement with the three close pK_a values 9.9,

(31) An additional residual peak of 0.5 e^- (from now on referred to as P) in the vicinity of W1 was observed with the following characteristics: d(P−W1) = 0.890 Å, d(P−W2) = 1.849 Å, (W1−P−W2) = 164(1)°. They were consistent with P being a proton from W1 (HW1), W1 being in a strong hydrogen bond with W2 through HW1.

(32) In the case of Fe(III): per two iron(III) (2 × (+3)), 4 oxygen {O(W1), O(W2i-iii)} (4 × (−2)), 6 imidazolate (6 × (−1)), and 1 PF_6^- (−1) are accounted. It requires 9 H+ to achieve neutrality.In the case of Fe(II): per two iron(II) (2 × (+2)), 4 oxygen {O(W1), O(W2i-iii)} (4 × (−2)), 6 imidazolates (6 × (−1)), and 3 PF_6^- (3 × (−1)) are accounted. It requires 13 H+ to achieve neutrality.

(33) In the case of $(Fe(II)(L1H_3))$, we noted a very insoluble black precipitate formation at intermediate pH when the experiment was done in anaerobic conditions. The IR spectrum is in agreement with a mixed compound formed by self-assemblage of protonated and deprotonated iron(II) complexes in 1/1 ratio. A similar type of layout has been recently published in the case of a 2-Me-imidazol-4-yl Fe(II) compound (see ref 14).

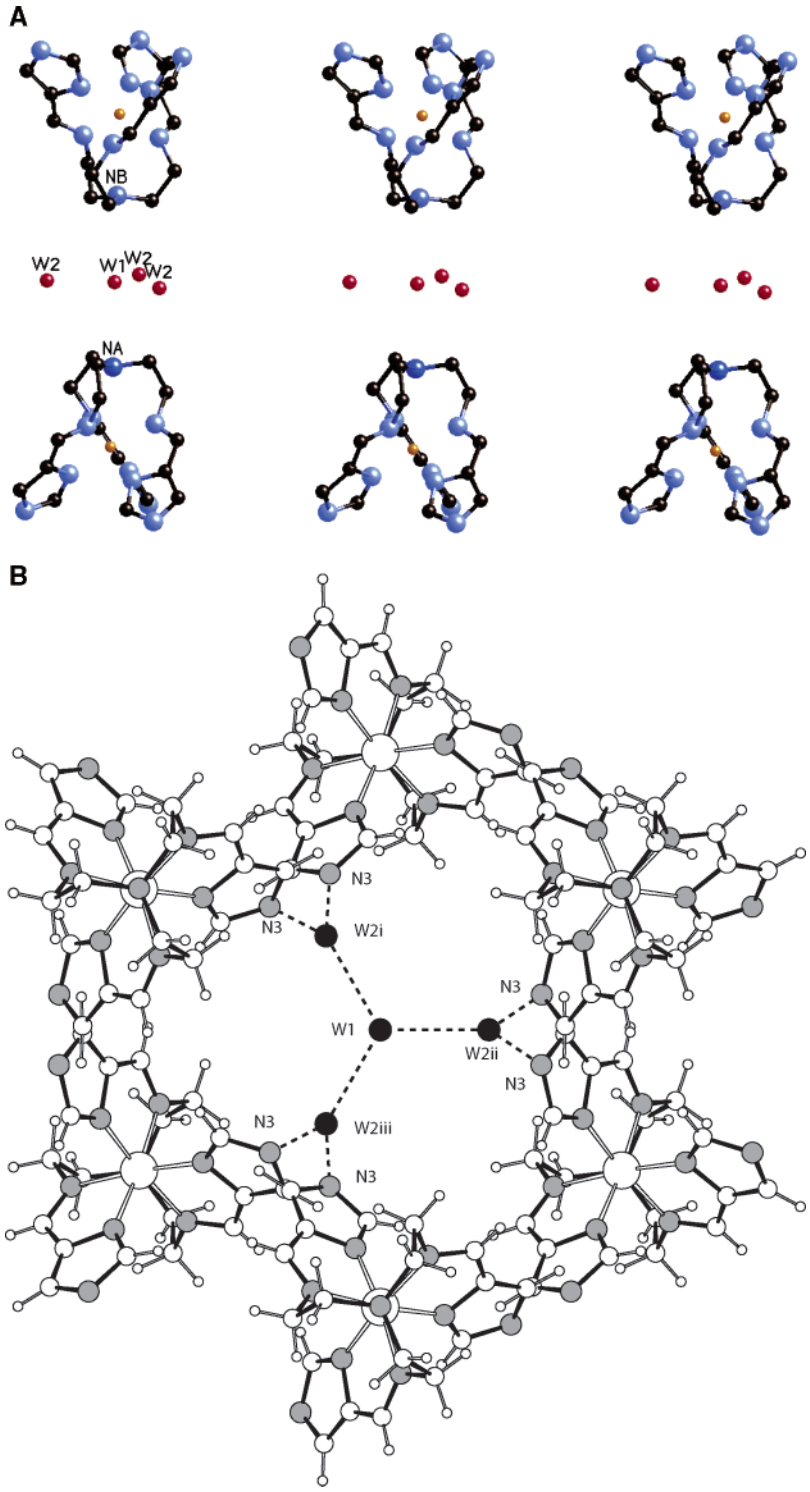

Figure 4. Water in the structure of $[Fe(III)(L1)]^0$ and organization of the network of cationic units around the "four-oxygen" units. (A) [Fe(III)(L1)] partial view of the capped structure (*c*-axis is vertical). Two layers {(AB)−W−(AB)′} are shown. For clarity, only A complexes (capped down) from the lower layer (AB) and B complexes (capped up) from the upper layer (AB)′ are shown (see also Scheme 3). Hydrogen bonds between water and $N_{imidazole}$ involve the hidden units and are shown in Figure 4B. (B) $[Fe(III)(L1)]^0$ view down the *c*-axis. Layout around one (W1, W2i−iii) unit. Sublayer A′ (above): iron hidden by N-tripod. Sublayer B (below): iron and N-tripod apparent (see text).

8.5, 7.3. Between pH 5.5 and 2.5, two new isobestic points appeared (435 and 595 nm), corresponding to the pK_a at 4.4.

This titration procedure could be reproducibly repeated (HCl then NaOH etc.) at least four times.

Iron(III)L2. The potentiometric titration of $[Fe(III)(L2)]^0$ with HCl showed a single equivalence for three protons with pK_a values of 7, 7.5, 8.8 (simulation, see Experimental Section). Due to the poor stability in aqueous acidic medium of the $[Fe(III)(L2H_3)]^{3+}$, the titration was not carried on at pH lower than 5.

Iron(II)L2. To avoid oxidation of iron(II) in iron(III), the titration of $[Fe(II)(L2H_3)]^{2+}$ was done with NaOH (0.09 mol L^{-1})/ascorbate (0.01 mol L^{-1}) or under anaerobic conditions. A single equivalence was observed for 2 protons with two

Scheme 3. Schematic Layout for the L1 Series

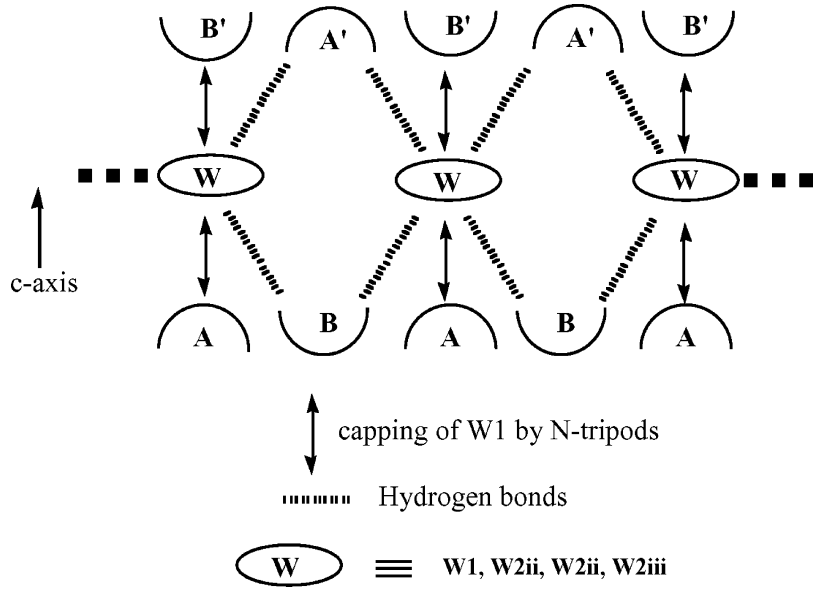

Scheme 4. Hydrogen Bond Network in L1 Series, Schematic View[a]

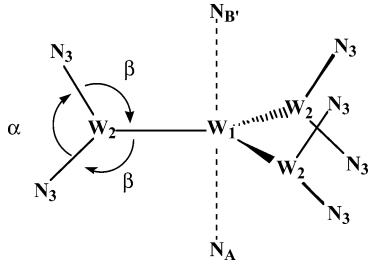

[a] See Table 3 for angles and distances.

Scheme 5. 4-Imidazole (A) versus 2-Imidazole (B)

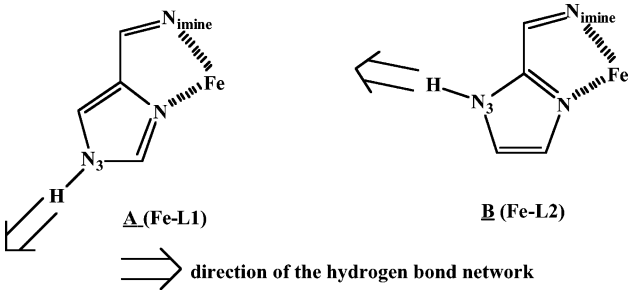

Table 3. (W1−W2ii−iii) Geometry in the L1 Series

	$[Fe(II)(L1H_3)](PF_6^-)_{1.5}$-$(H_7O_4^-)_{0.5}$ (orange)	$[Fe(III)(L_1)](PF_6^-)_{0.5}$-$(H_9O_4^+)_{0.5}$ (blue)
angles (deg)		
α	114(1)	121(1)
β	123(1)	120(1); 119(1)
distances (Å)		
W1−N3	5.097(16)	4.673(7); 4.647(7)
W2−N3	2.967(17)	2.682(6); 2.683(6)
W1−W2	2.810(16)	2.714(7)
W1−$N_{B'}$	3.810(3)	3.33(1)

pK_a values of 8.4, 9.5. As only two protons were measured, it suggests that, for the $[Fe(II)(L2H)]^0$ neutral form, deprotonation should be difficult (see below in part C). The potentiometric titration of $[Fe(II)(L2H_3)]^{2+}$ with HCl showed an equivalence for 1 proton exhibiting a pK_a of 3.1.

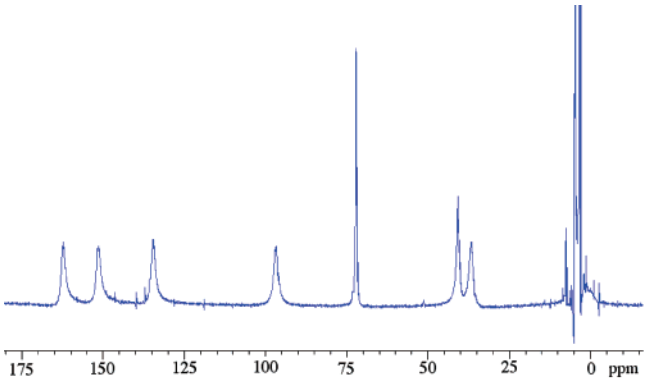

Figure 5. NMR spectrum of $[Fe(II)(L2H_3)]^{2+}(PF_6^-)(Cl^-)$ in MeOD.

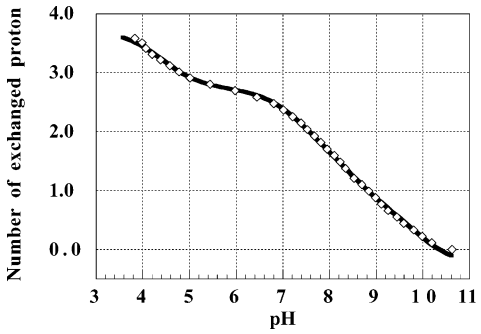

Figure 6. Exchanged proton (*x*, see definition in Experimental Section) as a function of pH starting from $[Fe(III)(L1)]^0$ solution in MeOH/H_2O (2/1) by HCl addition. For the sake of clariy, only 50% of the experimental data are presented (◇, experimental data; —, simulated data, see Experimental Section).

These pK_as are collected in Table 4. As expected, imidazole bound to iron(III) is found to be more acidic than that bound to iron(II). The two pK_as—3.1 for $[Fe(II)(L2H_3)]^{2+}$ and 4.4 for $[Fe(III)(L1H_3)]^{3+}$—are unusual. They might be assigned to the tripodal amine. The low basicity of this nitrogen could be due to its geometry being either "in" or "planar"[34] (see Scheme 6) with a hindered lone pair.

C. Redox Potentials. The variation of redox potentials Fe(III)/Fe(II) upon protonation−deprotonation of the coor-

Scheme 6. Schematic Representation of "In," "Planar," and "Out" Geometry for the N-Tripodal Ligand

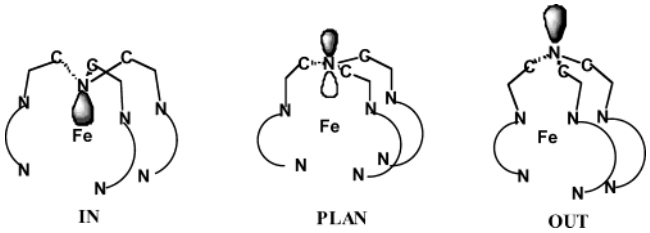

Table 4. Calculated pK_as[a]

ligand	DO_{Fe}	pK_{a1}	pK_{a2}
L1	Fe(III)	4.4	7.3; 8.5; 9.9
	Fe(II)	3.6	nd[c]
L2	Fe(III)	nd[b]	7; 7.5; 8.8
	Fe(II)	3.1	8.4; 9.5

[a] Each pK_a corresponds to one exchanged proton. [b] Not determined because $[Fe(III)(L2H_3)]^{3+}$ has not been isolated. [c] Not determined because of precipitation.[33]

Table 5. Half-Wave Potentials in MeOH/H_2O (2/1) (mV/SCE)

ligand of the Fe(II) or Fe(III) complex	pH_{measd}	$E_{1/2}$	$E_a - E_c$	couples
L1	5	366	68	$[Fe(III)(L1H_3)]^{3+}/[Fe(II)(L1H_3)]^{2+}$
L1	10.7	−359.5	95	$[Fe(III)(L1)]^0/[Fe(II)(L1H)]^0$
L2	4	451	109	$[Fe(III)(L2H_3)]^{3+}/[Fe(II)(L2H_3)]^{2+}$
L2	10.1	−374	76	$[Fe(III)(L2)]^0/[Fe(II)(L2H)]^0$

dinated ligand L has been investigated in both DMSO and CH_3OH/H_2O. It showed that the L−Fe(III)/L−Fe(II) potential can be tuned by protonation state.

Cyclic voltammograms (CVs) were recorded in both MeOH/H_2O (2/1) and DMSO for five of the compounds (namely, $[Fe(II)(L1H_3)]^{2+}$, $[Fe(II)(L2H_3)]^{2+}$, $[Fe(III)(L1H_3)]^{3+}$, $[Fe(III)(L1)]^0$, and $[Fe(III)(L2)]^0$). They showed quasi-reversible waves. Corresponding potentials are given in Tables 5 and 6. It was possible to switch from the acidic-couple wave to the basic-couple wave upon base addition (NaOH or methanolate). It was done in CH_3OH/H_2O (2/1) and in DMSO both with $[Fe(II)(L1H_3)]^{2+}$, $[Fe(III)(L1H_3)]^{3+}$, and $[Fe(II)(L2H_3)]^{2+}$. Similarly, it was possible to switch from the basic-couple wave to the acidic-couple wave upon acid addition (HCl, in DMSO and CH_3OH/H_2O (2/1)) in the case of both $[Fe(III)(L1)]^0$ and $[Fe(III)(L2)]^0$. In Figure 7, it is exemplified in the case of $[Fe(III)(L2)]^0$ upon acid addition (HCl) in MeOH/H_2O (2/1).

Assignment of the Redox Couples. In CH_3OH/H_2O (2/1). In the case of the L2 series, $[Fe(II)(L2H)]^0$, $[Fe(II)(L2H_3)]^{2+}$, and $[Fe(III)(L2)]^0$ have been isolated in the solid state, and potentiometric titration showed that in CH_3OH/H_2O (2/1) only 2 protons could be removed from $[Fe(II)(L2H_3)]^{2+}$. This indicated that the third deprotonation of $[Fe(II)(L2H_3)]^{2+}$ was difficult in this medium (CH_3OH/H_2O (2/1)). In the case of $[Fe(III)(L2)]^0$, three protons could be added (see the three pK_as above in B). In this medium, the acidic couple is $[Fe(III)(LH_3)]^{3+}/[Fe(II)(LH_3)]^{2+}$ and the basic couple is $[Fe(III)(L)]^0/[Fe(II)(LH)]^0$.

In DMSO. Upon base addition in $[Fe(II)(L2H_3)]^{2+}$ (10^{-3} mol L^{-1}), shifts of half-wave potential were recorded. Two titrations were followed by cyclic voltammetry, the first one using Et_3N and the second one using tBuOK. With tBuOK, a several-step deprotonation was observed (see Figure 8). At 2 equiv of tBuOK, a large wave with a half-wave potential at ca. −315 mV (/SCE) was recorded. At 3 equiv and above, a wave at −450 mV/SCE ($\Delta E_{a-c} = 85$ mV) was recorded. This potential corresponds to the $E_{1/2}$ measured in the case of $[Fe(III)(L2)]^0$ in DMSO (see Table 6). In the case of the titration with Et_3N (results not shown), the final wave (at 4 equiv) was at $E_{1/2} = -315$ mV/SCE. This indicates that with the weak base Et_3N, only two protons can be removed. With tBuOK it was possible to remove sequentially 2 protons (at 2 equiv of tBuOK) and a third one (at 3 equiv of tBuOK) producing $[Fe(II)(L2)]^-$. This is in agreement with what has been described in B. A similar phenomenon has been obtained with the L1 series ($E_{1/2}$ (2 equiv of tBuOK) = −350 mV/SCE; $E_{1/2}$ (3 equiv of tBuOK) = −445 mV/SCE).

In DMSO, the acidic couple is $[Fe(III)(LH_3)]^{3+}/[Fe(II)(LH_3)]^{2+}$ and the basic couple is $[Fe(III)(L)]^0/[Fe(II)(L)]^-$. According to p$K_a$s, the intermediate couple ($E_{1/2}$ = −315 mV for L2 and = −350 mV for L1) should be $[Fe(III)(L)]^0/[Fe(II)(LH)]^0$.

The two species $[Fe(II)(L2)]^-$ (purple) and $[Fe(II)(L1)]^-$ (pink) could be characterized by UV−vis spectroscopy (see Experimental Section). These species have also been obtained by reaction with superoxide (see D.2).

A difference of half-wave potentials $E_{1/2}$(Fe(III)/Fe(II)) was observed between the acidic and the basic forms. In CH_3OH/H_2O (2/1), $\Delta E_{1/2} = E_{1/2(deprot)} - E_{1/2(prot)}$ of −725.5 mV for L1 and of −825 mV for L2. In DMSO, $\Delta E_{1/2} = E_{1/2\ (deprot)} - E_{1/2(prot)}$ of −823 for L1 and −937 mV for L2. The deprotonation thus induces a negative shift of the potential.[3,4,6] This is consistent with an increase of the electronic density on the ligand which stabilizes the higher oxidation state iron(III).

In DMSO, three protons could be exchanged between acidic $[Fe(II/III)(LH_3)]^{2+/3+}$ and basic forms $[Fe(II/III)(L)]^{-1/0}$. It corresponds to a shift of −275 mV per proton upon deprotonation in the case of L1. In the case of L2, it corresponds to a shift of −312 mV per proton. The order of magnitude is consistent with the literature. For example, a shift of −350 mV due to imidazole deprotonation has been reported by Quinn et al. for an iron−porphyrin with axial imidazole.[3] An average shift of −300 mV has been reported by Haga et al. for a dimeric ruthenium complex of 2,2′-bis-(2-pyridyl)bibenzimidazole, with very different shifts, between −110 and −320 mV per deprotonated imidazole, depending on the oxidation state of the Ru and/or of the starting protonation state.[4] In the case of 2,6-diimidazolylpyridine iron(II) and iron(III) complexes, a shift of −345 mV per proton has been reported upon deprotonation.[6]

D. Reactivity with Dioxygen and with Superoxide Anion. 1. Conversion from $[Fe(II)(L1H_3)]^{2+}$ to $[Fe(III)(L1)]^0$: Protonation State and Reactivity with Dioxygen.

(34) Morgenstern-Badarau, I.; Lambert, F.; Renault, J. P.; Cesario, M.; Maréchal, J.-D.; Maseras, F. *Inorg. Chim. Acta* **2000**, *297*, 338−350.

Table 6. Half-Wave Potentials in DMSO (mV/SCE)

starting from:	$E_{1/2}$	$E_a - E_c$	couples
$[Fe(III)(L1H_3)]^{3+}$ or $[Fe(II)(L1H_3)]^{2+}$ [a]	378	89	$[Fe(III)(L1H_3)]^{3+}/[Fe(II)(L1H_3)]^{2+}$
$[Fe(III)(L1H_3)]^{3+}$, 2 equiv of tBuOK or excess Et_3N	−350	large	$[Fe(III)(L1)]^0/[Fe(II)(L1H)]^0$
$[Fe(III)(L1)]^0$ or $[Fe(III)(L1H_3)]^{3+}$, 3 equiv of tBuOK	−445	100	$[Fe(III)(L1)]^0/[Fe(II)(L1)]^-$
$[Fe(II)(L2H_3)]^{2+}$	480	103	$[Fe(III)(L2H_3)]^{3+}/[Fe(II)(L2H_3)]^{2+}$
$[Fe(III)(L2H_3)]^{3+}$, 2 equiv of tBuOK or excess Et_3N	−315	large	$[Fe(III)(L2)]^0/[Fe(II)(L2H)]^0$
$[Fe(III)(L2)]^0$ or $[Fe(III)(L2H_3)]^{3+}$, 3 equiv of tBuOK	−455	97	$[Fe(III)(L2)]^0/[Fe(II)(L2)]^-$

[a] As expected, CVs showed the same wave starting from either $[Fe(III)(L1H_3)]^{3+}$ or $[Fe(II)(L1H_3)]^{2+}$.

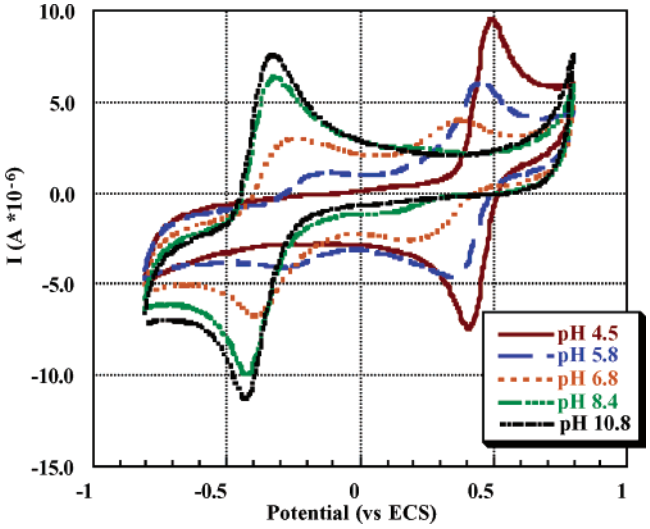

Figure 7. (Fe(III)/Fe(II)) potential for L2 with pH variation in MeOH/H_2O (2/1). $[Fe(III)(L2)]^0$ (10^{-3} mol L^{-1}), KCl (0.1 mol L^{-1}) as supporting electrolyte. "pH" is the pH directly measured in the electrochemical cell.

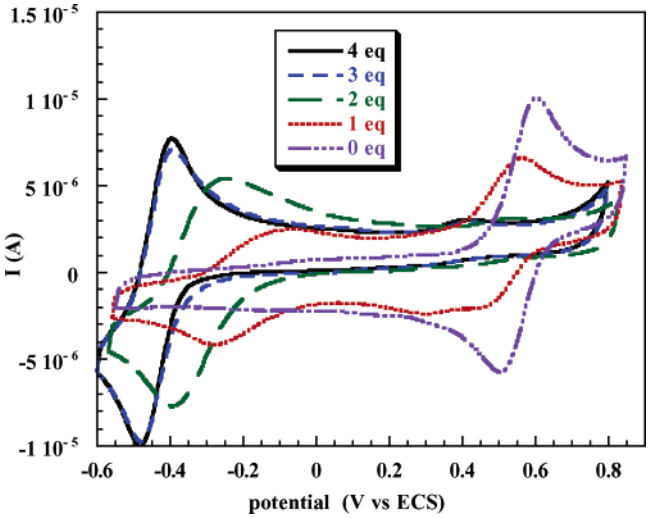

Figure 8. (Fe(III)/Fe(II)) potential for L2 with addition of successive equivalents of tBuOK. $[Fe(II)(L2H_3)]^{2+}$ (10^{-3} mol L^{-1}), NBu_4PF_6 (0.1 mol L^{-1}) as supporting electrolyte.

When $[Fe(II)(L1H_3)]^{2+}$ was titrated by NaOH under aerobic conditions, deprotonation was associated with oxidation of iron(II) in iron(III), as suggested by the color going from orange to blue. Spectral changes upon pH increase were recorded by UV−vis spectroscopy (see Figure 9). Three isobestic points (* in Figure 9) were obtained at 267, 412, and 497 nm. At high pH, the spectrum was identical to that of the $[Fe(III)(L1)]^0$ complex. This coupled acidobasic/air-oxidation reaction was characterized by an apparent pK_a [Fe-

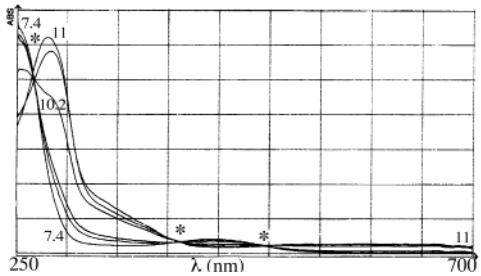

Figure 9. Electronic spectra in the L1 series starting from $[Fe(II)(L1H_3)]^{2+}$ at low pH. pH was increased by NaOH addition (labels refer to pH) (* = isobestic points).

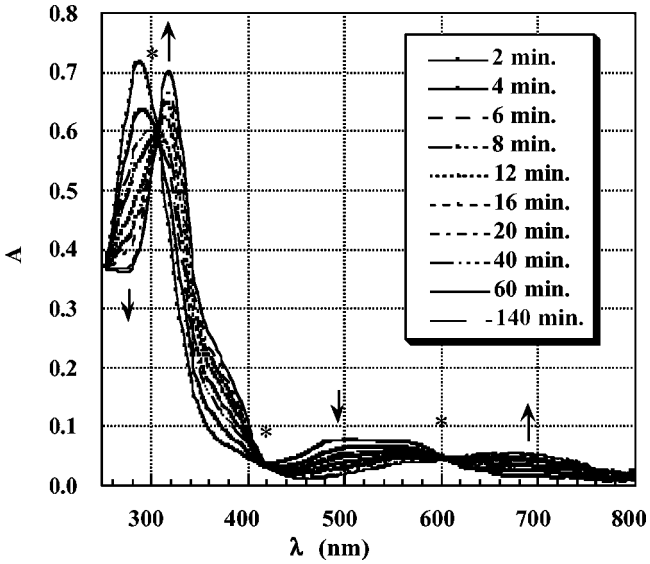

Figure 10. UV−visible spectra of $[Fe(II)(L2H_3)]^{2+}$ (2.5×10^{-5} mol L^{-1}) oxidation with O_2 in basic medium (MeO/H_2O (2/1), pH = 9), (* = isobestic points).

(II)$(L1H_3)]^{2+}$/$[Fe(III)(L1)]^0$ close to 9. It should be noted that a transient pink color and a precipitate appeared ($[Fe(II)(L1H)]^0$). The solution turned blue ($[Fe(III)(L1)]^0$) as the precipitate redissolved. This suggests that the kinetics of the aerobic oxidation is slow with regard to proton exchange. The same observations were made with the L2 series, but with no precipitation. The iron(II) complexes presented here are oxidized at high pH by dioxygen. In order to test them as SOD mimics, it is thus important to estimate the kinetics of this oxidation as it could perturb such a study.

The aerobic oxidation of $[Fe(II)(L2H)]^0$ ($[O_2] \gg [[Fe(II)(L2H)]^0]$) was followed by UV−vis spectroscopy (see Experimental Section and Figure 10). Three isobestic points were observed (*). Apparent first-order kinetics were observed up to 1200 s at both 284 and 470 nm (see Figure 11). Corresponding k_{app} are reported in Table 7.

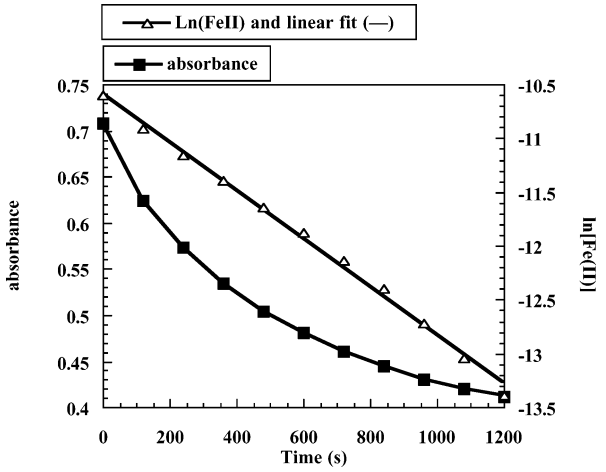

Figure 11. $[Fe(II)(L2H_3)]^{2+}$ (2.5×10^{-5}) oxidation with O_2 in basic medium (MeO/H_2O (2/1), pH = 9). Absorbance at 284 nm and ln [Fe(II)] versus time.

Table 7. Kinetics of Oxidation of $[Fe(II)(L2H_3)]^{2+}$ in Basic Medium

	pH 8	pH 9
$[O_2]_0$ (mol L^{-1})	3.8×10^{-4}	3.8×10^{-4}
$[Fe(II)(L2H_3)]_0$ (mol L^{-1})	2.5×10^{-5}	2.5×10^{-5}
k_{app} (mol^{-1} L s^{-1})	0.5×10^{-4}	22.4×10^{-4}

According to the redox potential measured for the protonated and deprotonated complex, the reaction involved the deprotonated form. It is in agreement with the observation of a slower reaction at pH 8 than pH 9. At pH 9, the oxidation was quick, and studies at higher pH require another setup than the quite simple one used here. However, at pH 8 and lower the reoxidation of iron(II) in iron(III) would not perturb superoxide reactivity studies.

2. Reactivity of Superoxide Anion with Complexes $[Fe(III)(L1)]^0$, $[Fe(III)(L2)]^0$, $[Fe(II)(L2H_3)]^{2+}$, and $[Fe(II)(L1H_3)]^{2+}$ in Anhydrous Medium. Superoxide reactivity of iron(II) complexes from similar ligands with N-protected imidazole (no exchangeable protons on the ligand) have been already described by us[22] and others,[30] and stable adducts [M−OO] have been proposed. It was interesting to study the reactivity of iron(II) derivatives bearing exchangeable protons. In DMSO solution of $[Fe(II)(L2H_3)]^{2+}$ (respectively $[Fe(II)(L1H_3)]^{2+}$), addition of excess equivalents of KO_2 induced the same species observed with excess tBuOK $[Fe(II)(L2)]^-$ (respectively $[Fe(II)(L1)]^-$) as shown by both cyclic voltammetry and UV−visible spectroscopy. O_2^- behaved in this system as a strong base, and no adducts were observed.

Successive equivalents of superoxide were added to a solution of $[Fe(III)(L2)]^0$. From 0 to 1 equiv, three isobestic points (293, 340, 389 nm) were observed. At 1 equiv, a purple solution was obtained which displayed a UV−vis spectrum identical to that of $[Fe(II)(L2)]^-$, and a cyclic voltammogramm with an $E_{1/2} = -455$ mV/SCE was recorded. At ratios O_2^-/complex higher than 1, no further changes were recorded. If the solution was then oxygenated, the initial spectrum of $[Fe(III)(L2)]^0$ was recovered within a few minutes. This cycle could be reproduced more than four times, without any noticeable modification. It indicates that the reaction $[Fe(III)(L2)]^0 + O_2^- = [Fe(II)(L2)]^- + O_2$ can be reversed. Similarly, addition of excess KO_2 in a solution of $[Fe(III)(L1)]^0$ led to $[Fe(II)(L1)]^-$, as characterized by UV−vis spectroscopy and CV. In these cases, O_2^- behaved as a reducing agent and no adducts were observed.

Conclusion

Two series of complexes were studied, involving L1 and L2. Their solid states have been described in detailed. Substitution of 2-imidazole for 4-imidazole was found far from being innocent.

The deprotonation pattern of these polyimidazole iron complexes has been investigated. Iron(III) complexes $[Fe(III)(LH_3)]^{3+}$ can be deprotonated three times (in MeOH/H_2O or in DMSO) with close pK_as. On the contrary, iron(II) complexes $[Fe(II)(LH_3)]^{2+}$ could only be deprotonated twice in MeOH/H_2O or in DMSO with Et_3N. In an aprotic medium (DMSO) with a strong base (tBuOK), a third deprotonation could be achieved, leading to $[Fe(II)(L)]^-$.

The redox potential of the Fe(III)/Fe(II) are dependent on the ligand. They were found to be tuned by the protonation state of the imidazole/imidazolate moiety. Upon deprotonation the redox potential of the Fe(III)/Fe(II) couple is lowered. In the case of the two series described here, shifts $\Delta E = E_{deprot} - E_{prot}$ from −270 to −320 mV were recorded per exchanged proton. Using UV−vis and cyclic voltammetry, we showed that the conversions between all the observed forms (iron(II), iron(III), imidazole, imidazolate) could be reversed. Several reducers (ascorbate and superoxide) and an oxidant (dioxygen) were used, either to synthesize the different complexes or to study their interconversions. It is summarized in Scheme 2. Preliminary studies of the reactivity with (i) superoxide and (ii) dioxygen have been described. Some exhaustive study is now in progress, involving these complexes and their manganese analogues.

An important point that was shown here is that interconversions are easy to control and they can be reversed several times. It is of interest for designing low dimensional metal materials as this can be used to finely control the oligopolymerization of metal units, as we and others already did.[8−10,13,17,18] Such a control is also of biological relevance. As a matter of fact, imidazole is quite often found in the coordination sphere of metal centers in biological systems or in the close vicinity and involved in a hydrogen bond network. The control over redox potentials by proton transfer, as exemplified here, can be an efficient way to tune back and forth the biological activity of metal centers.

Acknowledgment. This work was supported by the European Community (TMR Contract FMRX-CT980174).

Supporting Information Available: Tables of crystallographic information for the X-ray-characterized compounds and CIF file for (Fe(II)L2H). This material is available free of charge via the Internet at http://pubs.acs.org.

IC0498687